GEOLOGY | THE GEOLOGICAL SOCIETY OF AMERICA®

https://doi.org/10.1130/G46972.1

Manuscript received 6 September 2019
Revised manuscript received 15 January 2020
Manuscript accepted 28 January 2020

The effect of cooling during deformation on recrystallized grain-size piezometry

Hamid Soleymani[1]*, Steven Kidder[2], Greg Hirth[3] and Gordana Garapić[4]
[1]Department of Earth and Environmental Sciences, The Graduate Center, City University of New York, 365 5th Avenue, New York, New York 10016, USA
[2]Department of Earth and Atmospheric Sciences, City College of New York, City University of New York, 160 Convent Avenue, New York, New York 10031, USA
[3]Department of Earth, Environmental, and Planetary Sciences, Brown University, 324 Brook Street, Providence, Rhode Island 02912, USA
[4]Department of Geology, State University of New York at New Paltz, 1 Hawk Drive, New Paltz, New York 12561, USA

ABSTRACT

Most exposed middle- and lower-crustal shear zones experienced deformation while cooling. We investigated the effect of the strengthening associated with such cooling on differential stress estimates based on recrystallized grain size. Typical geologic ratios of temperature change per strain unit were applied in Griggs Rig (high pressure-temperature deformation apparatus) general shear experiments on quartzite with cooling rates of 2–10 °C/h from 900 °C to 800 °C, and a shear strain rate of ~2×10^{-5} s^{-1}. Comparisons between these "cooling-ramp" experiments and control experiments at constant temperatures of 800 °C and 900 °C indicated that recrystallized grain size did not keep pace with evolving stress. Mean recrystallized grain sizes of the cooling-ramp experiments were twice as large as expected from the final stresses of the experiments. The traditional approach to piezometry involves a routine assumption of a steady-state microstructure, and this would underestimate the final stress during the cooling-ramp experiments by ~40%. Recrystallized grain size in the cooling-ramp experiments is a better indicator of the average stress of the experiments (shear strains ≥3). Due to the temperature sensitivity of recrystallization processes and rock strength, the results may underrepresent the effect of cooling in natural samples. Cooling-ramp experiments produced wider and more skewed grain-size distributions than control experiments, suggesting that analyses of grain-size distributions might be used to quantify the degree to which grain size departs from steady-state values due to cooling, and thereby provide more accurate constraints on final stress.

INTRODUCTION

The stress magnitude in the crust, and its spatial and temporal variability, remains an active research area in geodynamics, earthquake mechanics, structural geology, and rock mechanics (e.g., Kohlstedt et al., 1995). One of the most widely used tools for quantifying stress magnitudes from middle-crustal rock samples is recrystallized grain-size piezometry (e.g., Twiss, 1977; Derby and Ashby, 1987; Shimizu, 1998; De Bresser et al., 2001). In laboratory experiments on quartz and other materials undergoing dislocation creep, there is a well-characterized inverse relationship between differential stress (referred to herein as "stress") and the size of new "dynamically recrystallized" grains produced during deformation (e.g., Fig. 1A). Experiments suggest that the relationship between flow stress and recrystallized grain size in quartz is independent of temperature, strain rate, and water content (Stipp et al., 2006). As currently implemented for geologic samples, for any mean recrystallized grain size, there is a single stress value that is assumed to represent some (unknown) final period of time when a rock was deformed at a relatively steady-state stress. Such stresses are often interpreted as representing peak stresses associated with ductile deformation near the brittle-ductile transition (e.g., Behr and Platt, 2011; Kidder et al., 2012). With the exception of samples strongly affected by seismic activity (e.g., Bestmann et al., 2012; Trepmann and Seybold, 2019), or subject to postdeformation annealing (e.g., Hacker et al., 1992), we are unaware of any significant previous evidence that supports or disproves this "steady-state" assumption. Hundreds of studies have used the recrystallized grain-size piezometer on various minerals and either implicitly or explicitly assumed that the recrystallized grain-size populations being measured resulted from long-term, steady-state deformation (e.g., Twiss, 1977; Kohlstedt and Weathers, 1980; Hacker et al., 1992; Dunlap et al., 1997; Hirth et al., 2001; Behr and Platt, 2011; Kidder et al., 2012). We explored the validity of the steady-state assumption by carrying out experiments in which cooling was imposed during deformation. Since cooling strengthens rocks in the ductile regime, stress gradually increased during the experiments. Deformation conditions spanned the range of temperature change per strain unit typical of natural shear zones (Fig. 2).

EXPERIMENTS

All of the experiments were carried out in general shear on samples synthesized from silica gel following the routine of Nachlas (2016). Three cooling-ramp experiments and three constant-temperature control experiments were conducted to a shear strain (γ) of ~4 (Figs. 1A and 1B). One additional deformation experiment was carried out to a relatively small strain (γ = 1.2) at 900 °C. Another sample (not included in Table 1) was quenched following annealing. This undeformed sample exhibited a

---

*E-mail: hsoleymani@gradcenter.cuny.edu

CITATION: Soleymani, H., Kidder, S., Hirth, G., and Garapić, G., 2020, The effect of cooling during deformation on recrystallized grain-size piezometry: Geology, v. 48, p. , https://doi.org/10.1130/G46972.1

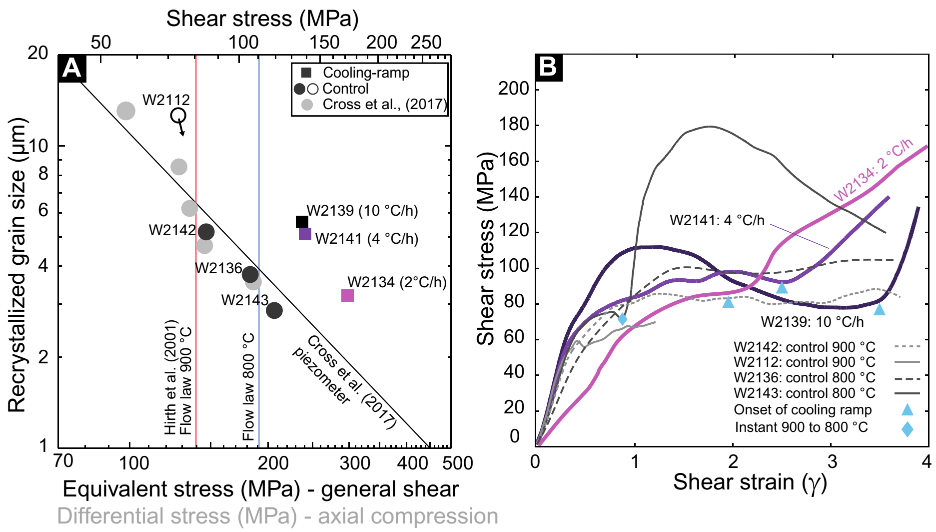

Figure 1. (A) Mean recrystallized grain size vs. stress from new constant-temperature experiments (black circles) and cooling-ramp experiments (squares). Recent calibration of recrystallized grain-size piezometer based on electron backscatter diffraction (black line) and associated constant-temperature data (gray circles) from Cross et al. (2017) are also shown. Stress values for ramp experiments are final stresses at time of quenching. Open circle (W2112) represents an early, non-steady-state condition through which most other experiments passed. Arrow on this sample indicates its evolution with strain toward the piezometer (e.g., as demonstrated by W2142). Predicted stress values based on the Hirth et al. (2001) flow law at 800 °C and 900 °C are in good agreement with control experiments. For comparison between experiments carried out in different geometries, measured values of shear stress (for general shear) were converted to equivalent stress (e.g., Paterson and Olgaard, 2000), which is equal to differential stress in axial compression (gray circles). Following this conversion, our control experiments plotted along the Cross et al. (2017) piezometer (cf. Heilbronner and Kilian, 2017). Standard errors on grain size are smaller than plotted symbols. (B) Shear stress versus shear strain for control experiments, and cooling-ramp experiments. Deformation temperatures are given above the mechanical data.

heterogeneous mixture of large (~100 µm) and small (~15 µm) grains (Fig. DR1c in the GSA Data Repository[1]). Stress versus strain curves are shown in Figure 1B. Shear strain rate ($\dot{\gamma}$) and confining pressure for all experiments were 2×10^{-5} s^{-1} and ~1.1 GPa, respectively. Control experiments were conducted at temperatures of 800 °C and 900 °C, or, in the case of experiment W2143, at 800 °C following deformation to $\gamma = 1.2$ at 900 °C (Fig. 1B). The experimental conditions at 900 °C fell close to the previously determined boundary between dislocation creep regimes 2 and 3 (Hirth and Tullis, 1992), and those at 800 °C were near the regime 1–2 boundary. Cooling-ramp experiments were conducted at a constant temperature of 900 °C prior to cooling. Cooling was imposed between temperatures of 900 °C and 800 °C at rates of 2, 4, and 10 °C/h, and the initiation of the cooling was timed so that a total strain of $\gamma \approx 4$ was achieved when temperatures reached 800 °C (Fig. 1B). Thus, slow cooling-ramp samples experienced more strain during cooling. Electron backscatter diffraction (EBSD) maps with a step size of 0.15 or 0.2 µm were analyzed with MTEX (https://mtex-toolbox.github.io/, Hielscher and Schaeben, 2008). Recrystallized grains were identified using the routine of Cross et al. (2017). Additional information on methods, sample preparation, and EBSD processing is provided in the Data Repository.

RESULTS

The samples showed expected strengths given the experimental conditions. Final sample strengths for the control samples were similar to those predicted by the Hirth et al. (2001) flow law (Fig. 1A). The two control experiments deformed near the regime 1–2 boundary followed different stress-strain paths but finished at a similar stress: Sample W2136 deformed at a relatively constant stress typical of regime 2, while sample W2143 exhibited strain hardening and then weakening, as typical of regime 1. The cooling-ramp samples also experienced strain hardening, as indicated by higher final stress values relative to those of the control experiments (Table 1; Fig. 1B).

Initial microstructures at the onset of cooling were inferred from the samples deformed at 900 °C. The mean grain size (all grains) of the sample deformed to $\gamma = 1.2$ (W2112) was ~15 µm. The recrystallized grain size of the larger strain 900 °C experiment (W2142) was 7 µm, consistent with the piezometer (Fig. 1A). Both of these samples exhibited abundant subgrains and interlobate grain boundaries (Fig. DR2) as expected for samples deformed near the regime 2–3 boundary (Hirth and Tullis, 1992). The 800 °C control samples also had abundant subgrains and grain boundaries marked by small-scale bulges (Fig. DR2). The cooling-ramp samples all showed a range of microstructures associated with relatively low-temperature and/or higher-stress deformation that were also evident in the

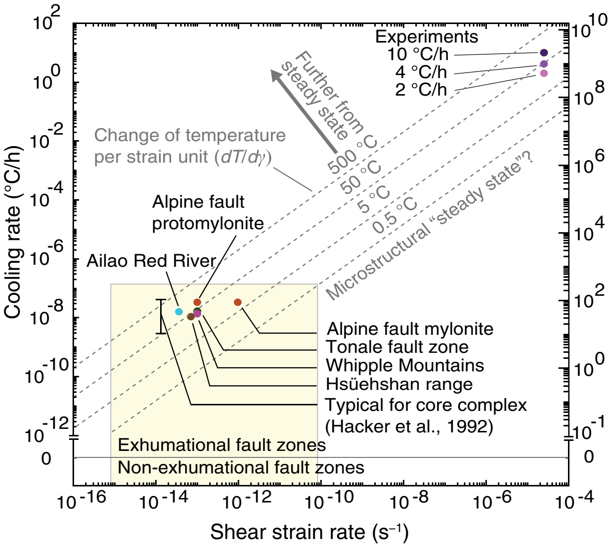

Figure 2. Log-log plot of cooling rate versus shear strain rate for cooling-ramp experiments and five well-studied naturally deformed zones (i.e., the Alpine fault in New Zealand, the Ailao Red River in Tibet, the Tonale fault in Italy, the Whipple Mountains in the USA, and the Hsüehshan range in Taiwan). Dashed lines are contours of equal cooling per increment of strain, and they suggest an equivalence between cooling-ramp experiments and typical geologic conditions. Beige box represents the ranges of strain rates and cooling rates estimated for natural samples. Due to evolution in strain rate and cooling rate with time, considerable variation at each locality is likely; e.g., as shown for the Alpine fault. "Steady state" refers to the situation where recrystallized grain size and stress fall along the piezometer (Fig. 1A). Natural data are from Hacker et al. (1992), Foster and John (1999), Wang et al. (2000), Norris and Cooper (2003), Stipp et al. (2004), Stockli et al. (2006), Sassier et al. (2009), Behr and Platt (2011), Kidder et al. (2012, 2013), and Fagereng and Biggs (2018).

---

[1] GSA Data Repository item 2020151, additional information on methods, sample preparation, and EBSD processing, is available online at http://www.geosociety.org/datarepository/2020/, or on request from editing@geosociety.org.

TABLE 1. SUMMARY OF THE EXPERIMENTAL CONDITIONS AND RESULTS

Sample number	W2112	W2142	W2139	W2141	W2134	W2143	W2136
Max temperature (°C)	900	900	900	900	900	800	800
Min temperature (°C)	–	–	800	800	800	–	–
Cooling rate (°C/h)	–	–	10	4	2	–	–
Shear strain, γ	1.2	3.7	3.9	3.5	4.0	3.6	3.6
Final shear stress, τ (MPa)	74	85	138	140	172	120	106
Avg τ (MPa)	73	82	93	99	108	144	97
Apparent τ (MPa)	51	90	85	89	118	124	107
Number of grains	954	626	796	612	2691	1833	1649
Median g.s (μm)	12.33	5.31	5.42	5.13	3.33	3.06	3.87
Mean g.s (μm)	15.21	7.03	7.79	7.26	5.10	4.06	5.26
Mean rxld g.s (μm)	13.48	5.39	5.92	5.49	3.49	3.23	4.06
Kurt g.s	6.39	7.44	4.17	5.66	22.55	26.16	9.03
Skew g.s	1.47	1.65	1.19	1.48	3.40	3.44	1.97
Skew g.s OL	0.75	0.79	0.92	0.90	1.01	0.85	0.86
NP skew g.s	0.24	0.22	0.29	0.28	0.29	0.25	0.27
Stdev g.s (μm)	6.25	3.52	4.13	3.80	2.92	1.96	2.59
GCV g.s	0.44	0.59	0.67	0.62	0.55	0.45	0.52
Mean GOS (°)	0.76	0.91	1.54	1.30	1.32	0.95	1.07
Median APR	1.57	1.65	1.94	1.66	1.69	1.56	1.75
J-index	1.76	3.49	3.14	3.20	1.95	2.09	3.14

Note: Abbreviations: Avg τ—the average shear stress calculated over the final 80% of the experiment; Apparent τ—shear stress calculated from recrystallized grains using Cross et al. (2017); g.s—grain size; rxld—recrystallized; Kurt—kurtosis; Skew g.s OL—skew calculated after outliers removed using Tukey's rule (Tukey, 1981); NP skew—nonparametric skew; Stdev—standard deviation; GCV—geometric coefficient of variation; GOS—grain orientation spread; APR—aspect ratio. J-index—measure of fabric strength. Mean grain size and recrystallized grain size are root mean square averages of grain diameters

800 °C control experiments, e.g., widespread bulges along grain boundaries, sweeping extinction, and deformation lamellae (Fig. DR3).

Grain size and grain-size distributions differed between the control and cooling-ramp experiments. Grain sizes (overall and recrystallized) of the cooling-ramp experiments correlated with the magnitude of cooling rate from values that grossly resembled the high-strain 900 °C control experiment (10 and 4 °C/h cooling rates) to values that resembled those of the 800 °C control experiments (2 °C/h cooling rate; Table 1). In addition, the grain-size distributions of the two fastest cooling-ramp samples (those furthest from "steady-state" in Fig. 2) were wider than the other experiments (Fig. 3). These larger grain-size spreads are visually evident from grain outline maps (Fig. 3B) showing a higher abundance of both coarse grains and fine grains for the faster cooling samples. Relative spread values, listed in Table 1, were quantified using the geometric coefficient of variation (GCV; Jensen et al., 2000), a size-independent measure of "standard deviation" of lognormally distributed data. GCV values increased with increased cooling rate; the value for the fastest cooling-ramp sample was 18% larger than the control experiment average. Nonparametric skew (NP skew = [mean – median]/stdev) was uniformly higher (~16%) in the cooling-ramp experiments relative to the controls. Standard skew values were heavily influenced by large outlier grains, but when the outliers were removed (Tukey, 1981) and skew was recalculated, the cooling-ramp experiments showed the largest asymmetry by this measure (11%–24% larger than control experiment average; Table 1).

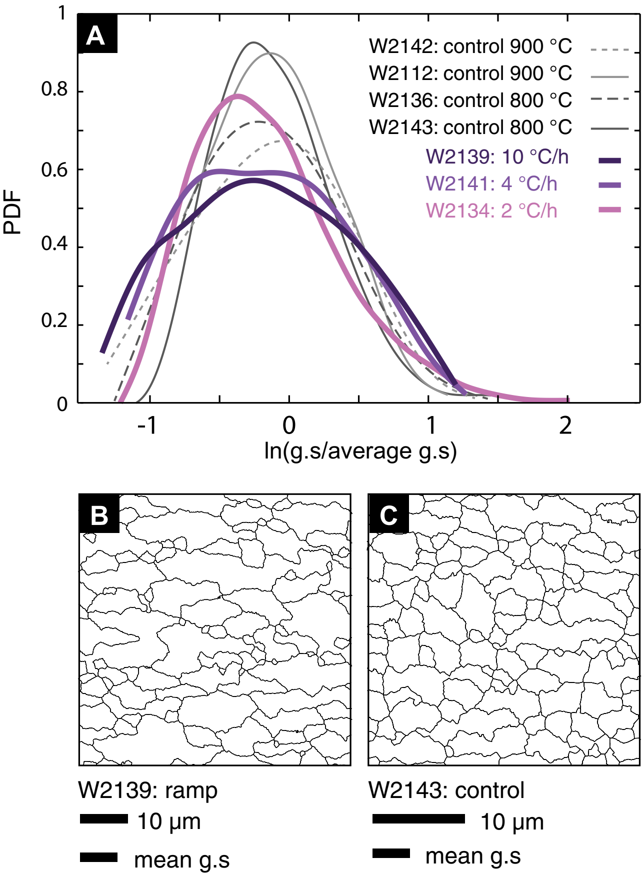

Figure 3. (A) Probability density function (PDF) of normalized grain size (g.s) for all grains. Nondimensional data were generated by taking log of each measured grain and then dividing each (log) grain size by the mean. Ramp experiments are plotted as thicker, colored lines. Plot demonstrates that fast ramp experiments (4 and 10 °C/h) had larger concentrations of small grains relative to other experiments. (B–C) Grain outlines from the cooling-ramp experiment (left) and control experiment (right). Scale of the images has been adjusted so that both images have same mean grain size. Compared to the control experiment, the cooling-ramp experiment has more numerous fine grains and coarse grains, and fewer grains near mean grain size.

Grain orientation spread (GOS), which measures distortion within grains, was also substantially higher in the cooling-ramp experiments (Table 1). Other microstructures, however, do not appear to have discriminated between the two types of experiments. For example, aspect ratios were highest in the experiment with a cooling rate of 10 °C/h, but they were not elevated relative to control experiments in the other cooling-ramp experiments, and intensity of lattice preferred orientation was similar between cooling-ramps and controls (Table 1).

DISCUSSION

Our results demonstrate that recrystallized grain size does not keep pace with increasing stress at deformation conditions scaled to the cooling rates of typical shear zones. The recrystallized grain sizes of the cooling-ramp experiments were nearly twice as large as would be predicted by the piezometer at final stress values (Fig. 1A). In turn, the final stresses of the experiments were ~40% larger than would be estimated based on traditional piezometry (Table 1).

These values may underestimate the true magnitude of the effect of cooling during deformation for natural samples, because at colder conditions, the underlying Arrhenius relationships may dictate (1) slower rates of microstructural change, and (2) larger differences in steady-state recrystallized grain size. Grain-size evolution models and experimental evidence indicate slower microstructural evolution rates at lower temperatures (e.g., Austin and Evans, 2009; Holtzman et al., 2018; Cross and Skemer, 2019). Additionally, owing to the Arrhenius relationship underlying the steady-state strength of quartz, a temperature change of 100 °C at geologic conditions corresponds to a larger percent change in steady-state recrystallized grain size than occurs in the laboratory (the change in 1/*T* due to a 100 °C shift is larger in the crust). Despite strain hardening in the ramp experiments, the relative shift required to maintain a steady-state grain size during a 100 °C temperature change is predicted to be roughly twice as large under natural conditions than in the cooling-ramp experiments (see the Data Repository). Any strain hardening occurring in natural shear zones would further accentuate this difference. In summary, relative to higher-temperature laboratory conditions, we anticipate that in nature, greater microstructural changes are required to keep pace with a temperature change, while at the same time, mechanisms for achieving such change are slowed. Such general predictions provide impetus for improving and applying grain-size evolution models (e.g., Austin and Evans, 2009; Holtzman et al., 2018) and clarifying potential effects of temperature differences on steady-state grain size (De Bresser et al., 2001).

Conventional grain-size piezometry is thus likely to underestimate peak stresses experienced by rocks exhumed through the brittle-ductile transition. Stresses calculated using the recrystallized grain-size piezometer should be considered minimum constraints on the final stress associated with dynamic recrystallization, unless it can be determined that deformation occurred at a relatively constant temperature. Such underestimated stresses could explain the discrepancy noted by Behr and Platt (2011) in the Whipple Mountains (southeastern California, USA) between geologic constraints on strain rate and flow law predictions based on piezometry. Recrystallized grain size is a better indicator of average stress during the entire deformation (Table 1) rather than peak stress.

Considering the likelihood that typical geologic rates of cooling and deformation significantly affect stress estimates from paleopiezometry, it is important, if possible, to distinguish microstructures formed under such conditions from those formed during steady-state flow. The results of our experiments suggest that the effects of cooling may be distinguished by wider and more asymmetric grain-size distributions (Table 1; Fig. 3). This result can be intuitively understood in a simplified model wherein recrystallized grains have a piezometrically stable size near the moment at which they form (e.g., Stipp et al., 2010; Kidder et al., 2012, 2016), and minimal growth occurs thereafter (e.g., Platt and De Bresser, 2017)—as increasingly smaller grains are generated over time, the left side of the grain-size distribution will inflate, leading to a rightward skew and wider distribution (Table 1; Fig. 3A). We hypothesize that these patterns could be more pronounced in natural settings involving larger amounts of strain and cooling over a larger range of temperature. If so, it might be possible to constrain the ratio of temperature change to strain rate (i.e., $dT/d\gamma$ contours in Fig. 2) from microstructural measurements. This could enable an estimate of peak stress by the application of some correction factor calibrated by experiments or predicted by modeling of grain-size distributions (e.g., Piazolo et al., 2002). Where cooling rate is known, estimates of $dT/d\gamma$ from a rock's microstructure would allow an estimation of strain rate (Fig. 2)—a rheologically significant quantity that is even less well constrained than stress (e.g., Fagereng and Biggs, 2018).

ACKNOWLEDGMENTS

We thank W.O. Nachlas for help with silica gel preparation, and L. Tokle, K. Okazaki, and N. Zhao for help running the experiments. This work was improved by comments of J.H.P. de Bresser, L. Morales, and an anonymous reviewer. The research was supported by U.S. National Science Foundation grant EAR-1524602 to Kidder.

REFERENCES CITED

Austin, N., and Evans, B., 2009, The kinetics of microstructural evolution during deformation of calcite: Journal of Geophysical Research: Solid Earth, v. 114, p. 1–22, https://doi.org/10.1029/2008JB006138.

Behr, W.M., and Platt, J.P., 2011, A naturally constrained stress profile through the middle crust in an extensional terrane: Earth and Planetary Science Letters, v. 303, p. 181–192, https://doi.org/10.1016/j.epsl.2010.11.044.

Bestmann, M., Pennacchioni, G., Nielsen, S., Göken, M., and De Wall, H., 2012, Deformation and ultrafine dynamic recrystallization of quartz in pseudotachylyte-bearing brittle faults: A matter of a few seconds: Journal of Structural Geology, v. 38, p. 21–38, https://doi.org/10.1016/j.jsg.2011.10.001.

Cross, A.J., and Skemer, P., 2019, Rates of dynamic recrystallization in geologic materials: Journal of Geophysical Research: Solid Earth, v. 124, p. 1324–1342, https://doi.org/10.1029/2018JB016201.

Cross, A.J., Prior, D.J., Stipp, M., and Kidder, S., 2017, The recrystallized grain size piezometer for quartz: An EBSD-based calibration: Geophysical Research Letters, v. 44, p. 6667–6674, https://doi.org/10.1002/2017GL073836.

De Bresser, J.H.P., Ter Heege, J.H., and Spiers, C.J., 2001, Grain size reduction by dynamic recrystallization: Can it result in major rheological weakening?: International Journal of Earth Sciences, v. 90, p. 28–45, https://doi.org/10.1007/s005310000149.

Derby, B., and Ashby, M.F., 1987, On dynamic recrystallisation: Scripta Metallurgica, v. 21, p. 879–884, https://doi.org/10.1016/0036-9748(87)90341-3.

Dunlap, W.J., Hirth, G., and Teyssier, C., 1997, Thermomechanical evolution of a ductile duplex: Tectonics, v. 16, p. 983–1000, https://doi.org/10.1029/97TC00614.

Fagereng, Å., and Biggs, J., 2018, New perspectives on 'geological strain rates' calculated from both naturally deformed and actively deforming rocks: Journal of Structural Geology, v. 125, p. 1–11, https://doi.org/10.1016/j.jsg.2018.10.004.

Foster, D.A., and John, B.E., 1999, Quantifying tectonic exhumation in an extensional orogen with thermochronology: Examples from the southern Basin and Range Province, *in* Ring, U., et al., eds., Exhumation Processes: Normal Faulting, Ductile Flow and Erosion: Geological Society [London] Special Publication 154, p. 343–364, https://doi.org/10.1144/GSL.SP.1999.154.01.16.

Hacker, B.R., Yin, A., Christie, J.M., and Davis, G.A., 1992, Stress magnitude, strain rate, and rheology of extended middle continental crust inferred from quartz grain sizes in the Whipple Mountains, California: Tectonics, v. 11, p. 36–46, https://doi.org/10.1029/91TC01291.

Heilbronner, R., and Kilian, R., 2017, The grain size(s) of Black Hills quartzite deformed in the dislocation creep regime: Solid Earth, v. 8, p. 1071–1093, https://doi.org/10.5194/se-8-1071-2017.

Hielscher, R., and Schaeben, H., 2008, A novel pole figure inversion method: Specification of the MTEX algorithm: Journal of Applied Crystallography, v. 41, p. 1024–1037, https://doi.org/10.1107/S0021889808030112.

Hirth, G., and Tullis, J., 1992, Dislocation creep regimes in quartz aggregates: Journal of Structural Geology, v. 14, p. 145–159, https://doi.org/10.1016/0191-8141(92)90053-Y.

Hirth, G., Teyssier, C., and Dunlap, J.W., 2001, An evaluation of quartzite flow laws based on comparisons between experimentally and naturally deformed rocks: International Journal of Earth Sciences, v. 90, p. 77–87, https://doi.org/10.1007/s005310000152.

Holtzman, B.K., Chrysochoos, A., and Daridon, L., 2018, A thermomechanical framework for analysis of microstructural evolution: Application to olivine rocks at high temperature: Journal of Geophysical Research: Solid Earth, v. 123, p. 8474–8507, https://doi.org/10.1029/2018JB015613.

Jensen, J., Lake, L.W., Corbett, P.W.M., and Goggin, D., 2000, Statistics for Petroleum Engineers and Geoscientists, v. 2: Houston, Texas, Gulf Professional Publishing, 362 p.

Kidder, S., Avouac, J.-P., and Chan, Y.-C., 2012, Constraints from rocks in the Taiwan orogen on crustal stress levels and rheology: Journal of Geophysical Research: Solid Earth, v. 117, B09408, https://doi.org/10.1029/2012JB009303.

Kidder, S., Avouac, J.P., and Chan, Y.C., 2013, Application of titanium-in-quartz thermobarometry to greenschist facies veins and recrystallized quartzites in the Hsüehshan range, Taiwan: Solid Earth, v. 4, p. 1–21, https://doi.org/10.5194/se-4-1-2013.

Kidder, S., Hirth, G., Avouac, J.-P., and Behr, W., 2016, The influence of stress history on the grain size and microstructure of experimentally deformed quartzite: Journal of Structural Geology, v. 83, p. 194–206, https://doi.org/10.1016/j.jsg.2015.12.004.

Kohlstedt, D.L., and Weathers, M.S., 1980, Deformation-induced microstructures, paleopiezometers, and differential stresses in deeply eroded fault zones: Journal of Geophysical Research: Solid Earth, v. 85, p. 6269–6285, https://doi.org/10.1029/JB085iB11p06269.

Kohlstedt, D.L., Evans, B., and Mackwell, S.J., 1995, Strength of the lithosphere: Constraints imposed by laboratory experiments: Journal of Geophysical Research: Solid Earth, v. 100, p. 17587–17602, https://doi.org/10.1029/95JB01460.

Nachlas, W.O., 2016, Precise and accurate doping of nanoporous silica gel for the synthesis of trace element microanalytical reference materials: Geostandards and Geoanalytical Research, v. 40, p. 505–516, https://doi.org/10.1111/ggr.12120.

Norris, R.J., and Cooper, A.F., 2003, Very high strains recorded in mylonites along the Alpine fault, New Zealand: Implications for the deep structure of plate boundary faults: Journal of Structural Geology, v. 25, p. 2141–2157, https://doi.org/10.1016/S0191-8141(03)00045-2.

Paterson, M.S., and Olgaard, D.L., 2000, Rock deformation tests to large shear strains in torsion: Journal of Structural Geology, v. 22, p. 1341–1358, https://doi.org/10.1016/S0191-8141(00)00042-0.

Piazolo, S., Bons, P.D., Jessell, M.W., Evans, L., and Passchier, C.W., 2002, Dominance of microstructural processes and their effect on microstructural development: Insights from numerical modelling of dynamic recrystallization, *in* De Meer, S., et al., eds., Deformation Mechanisms, Rheology and Tectonics: Current Status and Future Perspectives: Geological Society [London] Special Publication 200, p. 149–170, https://doi.org/10.1144/GSL.SP.2001.200.01.10.

Platt, J.P., and De Bresser, J.H.P., 2017, Stress dependence of microstructures in experimentally deformed calcite: Journal of Structural Geology, v. 105, p. 80–87, https://doi.org/10.1016/j.jsg.2017.10.012.

Sassier, C., Leloup, P.-H.H., Rubatto, D., Galland, O., Yue, Y., and Lin, D., 2009, Direct measurement of strain rates in ductile shear zones: A new method based on syntectonic dikes: Journal of Geophysical Research: Solid Earth, v. 114, B01406, https://doi.org/10.1029/2008JB005597.

Shimizu, I., 1998, Stress and temperature dependence of recrystallized grain size: A subgrain misorientation model: Geophysical Research Letters, v. 25, p. 4237–4240, https://doi.org/10.1029/1998GL900136.

Stipp, M., Fügenschuh, B., Gromet, L.P., Stünitz, H., and Schmid, S.M., 2004, Contemporaneous plutonism and strike-slip faulting: A case study from the Tonale fault zone north of the Adamello pluton (Italian Alps): Tectonics, v. 23, p. 1–23, https://doi.org/10.1029/2003TC001515.

Stipp, M., Tullis, J., and Behrens, H., 2006, Effect of water on the dislocation creep microstructure and flow stress of quartz and implications for the recrystallized grain size piezometer: Journal of Geophysical Research: Solid Earth, v. 111, B04201, https://doi.org/10.1029/2005JB003852.

Stipp, M., Tullis, J., Scherwath, M., and Behrmann, J.H., 2010, A new perspective on paleopiezometry: Dynamically recrystallized grain size distributions indicate mechanism changes: Geology, v. 38, p. 759–762, https://doi.org/10.1130/G31162.1.

Stockli, D.F., Brichau, S., Dewane, T.J., Hager, C., and Schroeder, J., 2006, Dynamics of large-magnitude extension in the Whipple Mountains metamorphic core complex: Geochimica et Cosmochimica Acta, v. 70, Supplement, p. A616–A616, https://doi.org/10.1016/j.gca.2006.06.1143.

Trepmann, C.A., and Seybold, L., 2019, Deformation at low and high stress-loading rates: Geoscience Frontiers, v. 10, p. 43–54, https://doi.org/10.1016/j.gsf.2018.05.002.

Tukey, J.W., 1981, Exploratory data analysis: Biometrical Journal (Biometrische Zeitschrift), v. 23, p. 413–414, https://doi.org/10.1002/bimj.4710230408.

Twiss, R.J., 1977, Theory and applicability of a recrystallized grain size paleopiezometer: Pure and Applied Geophysics (PAGEOPH), v. 115, p. 227–244, https://doi.org/10.1007/978-3-0348-5745-1_13.

Wang, P.-L., Lo, C.-H., Chung, S.-L., Lee, T.-Y., Lan, C.-Y., and Van Thang, T., 2000, Onset timing of left-lateral movement along the Ailao Shan–Red River shear zone: $^{40}Ar/^{39}Ar$ dating constraint from the Nam Dinh area, northeastern Vietnam: Journal of Asian Earth Sciences, v. 18, p. 281–292, https://doi.org/10.1016/S1367-9120(99)00064-4.

Printed in USA